Engineering model for rocket exhaust plumes verified by CFD results

By Carola BAUER[1)], Aaron KOCH[1)] Francesco MINUTOLO[1)] and Philippe GRENARD[2)]

[1)]*German Aerospace Centre (DLR), Space Launcher System Analysis (SART)*
Institute of Space Systems, Bremen, Germany
[2)]*ONERA, Paliseau, France*

An engineering model (EM) is under development that describes the propagation of a rocket exhaust plume after the nozzle exit. The aim of this EM is to allow a fast analysis of the structure of the plume and the exhaust species within the plume. The characteristics of the plume depend highly on the ambient conditions, which vary depending on the altitude. In particular, the ambient pressure plays a significant role. Therefore, the properties of the plume need to be investigated across multiple altitudes. CFD calculations have been performed for a few selected altitudes and several launchers. These results are used to verify the EM. As the CFD calculations for entire launchers are very time consuming to compute, the EM provides a quicker way to analyse the basic properties of the rocket plumes at a variety of altitudes.

Key Words: Engineering Model, CFD, Rocket Exhaust Plume, Gas Dynamics

Nomenclature

CFD	Computational Fluid Dynamics
SART	Space Launcher System Analysis
ONERA	Office National d'Études et de Recherches Aérospatiales
EM	Engineering Model
ATILA	Atmospheric Impact of Launchers
SRM	Solid rocket motor
HCl	Hydrogen chloride
Cl	Chlorine
Al_2O_3	Aluminium oxide, alumina

1. Introduction

As part of the ESA Clean Space Initiative, the study AtILa began in 2012 with the aim of obtaining information about the environmental impact of launchers on the atmosphere. Within this study, several companies and institutions are involved. To reach the aim, the characteristic parameters of the rocket exhaust plumes need to be known. This means that the beginning of the calculation process needs to start either at the combustion chamber, or at the latest at the nozzle exit.

The structure of the plume is complex, and it can be divided into three regions: near field, transition region and far field. In Figure 1 the scheme of the plume structure is displayed [1].

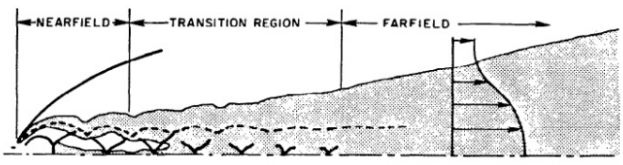

Figure 1: Scheme of the plume structure [1]

In this figure, it can be seen that the near field is close to the nozzle exit of the engine where the flow from inside the nozzle dominates the plume structure. In the transition region, however, mixing with the atmosphere increases whereas the core flow decreases and loses influence on the plume structure. In the far field, the core flow has vanished and thus, no longer plays a role, whilst the mixing with the ambient environment takes full effect.

Within the AtILa project, the near field is calculated with CFD computations for only selected altitudes. However, to obtain knowledge over a wider altitude range, an engineering model (EM) is under development. The purpose of this EM is not to replace the CFD, but to obtain information faster and over a wider range of altitudes.

The objective of this paper is to compare the first inviscid cell of the exhaust plume from the EM with CFD results for the VEGA launcher at specific altitudes.

2. Plume Structure

As mentioned before, the plume structure is complex. Due to this, it is worthwhile to provide an introduction into this subject. The plume structure itself does not depend on the fuel and oxidant, whilst the emissions of course do.

According to Simmons [2], the core flow from the nozzle exit can be divided into two sections: the inviscid inner core and the viscous outer core (mixing layer). Within the inviscid core, it is assumed that no chemical reactions occur [2].

Figure 2 presents a schematic of the near field plume structure. In this figure, it can also be seen that the mixing layer thickness increases with increasing distance from the nozzle exit. However, in the inviscid core, shocks and expansion waves occurs and thus, the flow structure is dominated by these gas dynamic characteristics.

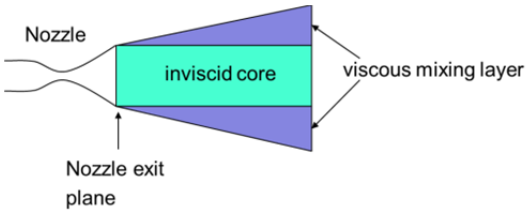

Figure 2: Schematic of the plume structure in the near field

The plume can be divided into the two parts mentioned above. The flow in the inviscid core is non-reacting in contrast to the mixing layer. In the mixing layer the flow is viscid and surrounds the core flow. The reactions take place by mixing with the ambient environment [2].

An additional set of reactions can occur in the viscous mixing layer, which is known as afterburning. The occurrence of afterburning, however, depends on the altitude. The chemical reaction which leads to afterburning occurs only when the oxygen concentration is high enough. Afterburning leads to higher temperatures in the mixing zone and thus, to infrared emissions, which can be observed [3].

The plume expands as the ambient pressure decreases, as the launch vehicle accelerates and rises through the atmosphere. The turbulent mixing also decreases as the relative velocity between the exhaust and the free stream decreases. Less mixing and a decreased temperature lead to a decrease in afterburning, and thus, observed emissions. The process of afterburning ends when the velocity of the vehicle is equal to the velocity of the exhaust. That means when the exhaust is released into the atmosphere with a relative velocity of zero [2].

Near Field

Lohn et al. [4] produced a schematic view of the plume structure (see Figure 3). In this figure, the flow exiting the nozzle generates at the nozzle lip expansion waves which are reflected at the plume boundary. Expansion waves only occur when the flow in the nozzle has a higher pressure than the ambient environment. When the pressure at the nozzle exit is smaller than the outside pressure, a shock occurs.

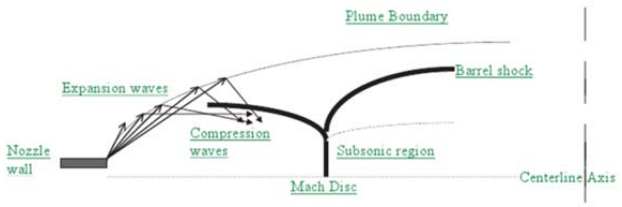

Figure 3: Flow structure of a supersonic single nozzle plume [4]

However, in most exhaust plumes the gas pressure at the nozzle exit is higher than the ambient pressure. This leads to an under-expanded jet. In order to attempt to match the ambient pressure, the plume will expand after the nozzle exit so that there will be expansion waves at the nozzle exit. These waves will propagate downstream to a point where the expansion waves intercept the ambient boundary, which has a constant pressure.

Due to reflections from the plume boundary, the expansion waves become compression waves, with the aim of matching the local pressure which is higher. The reflected compression waves merge further downstream because of the shape of the plume boundary. This merging leads to a barrel shock. If this barrel (or oblique) shock is strong, a normal shock (Mach disc) will appear on the centerline. A subsonic region after this Mach disc will occur. The pattern of barrel shock and Mach disk is driven by the ratio of the pressure at the exit and the ambient pressure. This pattern can repeat itself several times and in this case a diamond crystal shape pattern ("shock diamond") occurs. This shock diamond weakens with the mixing [4], i. e. the further away from the nozzle exit, the weaker the shock diamond.

Far field

When the pattern of barrel shocks ends, the far field begins. This means, that the mixing with the ambient environment dominates and the afterburning process can occur. After a while, the plume is completely mixed with the ambient environment and the plume is dispersed within the surrounding atmosphere. Smith et al. [5] summarized a series of studies, works with in-situ measurements, laboratory measurements and models for solid rocket motor (SRM) exhausts.

Afterburning

Some more words about the afterburning process in rocket exhaust plumes are necessary. As mentioned previously, afterburning processes occur when the plume mixes with the ambient atmosphere. However, the afterburning reactions depend on the altitude of the plume, because with increasing altitude, oxygen content of the atmosphere decreases [2]. The oxygen content is important because the fresh and unburnt oxygen is responsible for the further burning processes.

Furthermore, the afterburning process depends also on the degree of mixing. The less the plume mixes with the ambient environment, the more unlikely afterburning will occur. The end of the afterburning process is caused either by the altitude (and hence lack of oxygen) or when the velocity of the rocket matches the velocity of the exhaust [2].

Several previous investigations into afterburning have been conducted. Burke and Zittel [6] made laboratory measurements and investigated SRM exhausts under afterburning conditions. They simulated an altitude range of approx. 15 – 40 km, and they were especially interested in the behavior of HCl under stratospheric conditions.

Furthermore, laboratory measurements and computational models have been developed by other authors. However, the focuses of these studies have been different.

Brady et al. [7] developed a model to investigate the influence of time. They investigated the plume chemistry for a period of time of up to 1 day. Afterburning takes place at the beginning of the simulation and was taken into account. The authors used a plume dispersion and chemical kinetic model to specify the exhaust gases throughout the afterburning region of an SRM exhaust plume. The study's goal was to obtain knowledge about the physical characteristics and the chemical residue. Brady et al. also discovered that afterburning has a significant effect on the HCl conversion and thus, on local ozone depletion.

Alternatively, Denison et al. [8] developed a model to investigate the reactions of the plume with the ambient atmosphere. The authors conclude that afterburning can be a source of local ozone depletion. They also state that afterburning can convert HCl into Cl and other active chlorine containing species.

Already in the late 1970s, numerical simulations were conducted by Gomberg and Stewart [8]. Knowledge about afterburning in SRM plumes and the resulting chemical reactions were obtained through their simulations.

Leone and Turns [10] modeled afterburning in a rocket plume using two chemical kinetic systems. The authors compared their results concerning chlorine with the results from Gomberg and Stewart [8] and found them to be in good agreement.

To summarize the above mentioned references, the afterburning process is crucial for the impact of exhaust plumes on the atmosphere. However, to obtain more information about the influence of afterburning, further investigations on the near field plume are required. The near field plume structure is responsible for the mixing impact of the entire plume from the nozzle exit until the final dispersion of the plume within the ambient atmosphere, and thus this is the area which must be investigated.

3. Theory & Methods

Due to the inviscid core of the jet plume of an under-expanded nozzle, the theory of characteristics [11], which can be implemented in a fast computer program, is able to quickly calculate the main thermodynamic variables that characterize the flow in the first cell of the main core.

In particular, the first algorithm defines the shape of the *leading characteristic*. The second step is to evaluate the angle of expansion at the nozzle lips to delineate the contour of the plume, and lastly the characteristic network is modelled in order to cover the entire inviscid structure.

Approach

An example of a flow field that can be easily resolved by the method of characteristics is the one encountered at the exit of a sub-expanded nozzle.

Some considerations and assumptions must however be made to define the method of characteristics introduced in this work:

- The nozzle must always operate in an under-expanded regime.
- The effects of viscosity are neglected.
- The flow is considered isentropic.
- The jet is axisymmetric.
- The internal plume is considered dissolved by the viscous effects.

With these properties defined, the flow at the nozzle lips expands to the external pressure value due to expansion waves that interact with each other on the axis line forming new expansion waves. When these are reflected on the boundary layer they turn into compression waves

Determination of the *leading characteristic*

The *leading characteristic* in an under-expanded nozzle is the line that separates the internal plume into two main flow regions. The internal flow is called the zone of zero external influence, where flow properties strictly depend only on nozzle exit area properties. The external flow features, delimited by the jet boundary, are on the contrary driven by the external static pressure value. The ending point of that line is represented by its intersection with the axial centre line.

To calculate this line some input data must be known:

- Mach number at the nozzle exit
- Nozzle half-angle or angle of flow at nozzle lips
- Ratio of specific heats
- static pressure at nozzle exit
- static ambient pressure

The calculation of the *leading characteristic* strictly depends on the chosen type of nozzle configuration. However, within the AtILa study only conical nozzles are considered.

For conical nozzles, the *leading characteristic* is a curved line. This implies that all flow properties along this line change and therefore they must be calculated. In Figure 4, a sketch of a conical nozzle is shown, including all of the geometrical parameters needed as inputs for the calculation.

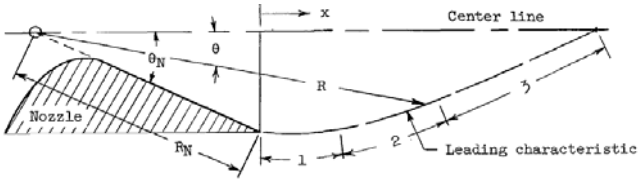

Figure 4: Sketch of leading characteristic of a conical nozzle [12]

To compute the Mach number at the edge point, the Prandtl-Meyer expansion has been used to show that at the nozzle exit, the flow direction is defined by the nozzle slope while at the centreline the flow returns to be parallel [12].

In Figure 5, a typical net of characteristics is shown. The different numbers indicate the different locations and thus, another calculation.

The different points in this figure can be identified as seen in Table 1. Knowledge of Point 1 (the nozzle lip) is crucial because all further calculations are based on this point's parameters.

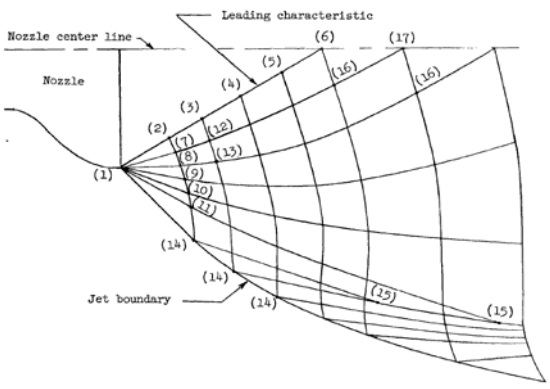

Figure 5: An expanded view of a typical characteristic net [12]

Table 1: Meaning of the point numbers in Figure 5

Point number	Meaning
1	Nozzle lip
2, 3, 4, 5	Input data points on leading characteristic
6	Last leading characteristic point, also 1st point on centre line
7 – 13	General points
14	Boundary point
15	Same family point (internal shock)
16	Point adjacent to centre line
17	Points on centre line

For the engineering model, the method of characteristics is applicable for the inner core flow of the exhaust plume until the occurrence of the Mach disk which defines the end of the first cell. However, to verify this method within the AtILA project, CFD computations are taken for different altitudes.

The application of the CEA code for simulation the afterburning process has to be applied at a certain location. The selection of the right location is important to get relevant thermodynamic and flow properties.

4. CFD results

For the VEGA launcher three calculations have been conducted for different altitudes: 18.7 km, 30 km, and 42 km.

The mesh used for VEGA computations was generated with GMSH [13] and consists of approximately 200 000 triangular cells. The geometry is 2D axisymmetric. The boundary conditions were chosen according to US standard atmosphere 1976 and trajectory points for the outer flow at the three altitudes computed. The chamber boundary condition was computed by means of the thermochemical equilibrium code OPHELIE. All wall boundaries are considered adiabatic. The CEDRE code [14] is used to compute the turbulent reactive and diphasic flow for these cases. The turbulence is considered through the use of a k-ω SST model (modified according to [15] for 2D axisymmetric flows) and the chemistry is modeled by a reaction scheme [16]. For the diphasic part (Al_2O_3 particles), the treatment is divided into the smallest particles (5% of the whole particle mass), which are treated as an equivalent gas species, while the largest particles (95% in mass) are treated using an Eulerian dispersed phase solver.

The main challenge of this approach was to choose an appropriate particle size distribution for alumina particles. A Dirac distribution was chosen, with a size corresponding to the expected value in the plume. As the fragmentation of these particles is not computed, the same distribution was imposed inside the combustion chamber. This led to difficulties in recovering a correct mass flow rate and chamber pressure simultaneously. The exchange between particles and gas phase are proportional to their surface area (to d^2) but the number of particles, for a fixed mass flow, is inversely proportional to their volume (to $1/d^3$). Thus, for a fixed mass flow, these effects integrated are linked to 1/d. As friction tends to slow down the gas and thermal exchange tends to heat the fluid during the acceleration of the fluid in the convergent nozzle (and thus reduce the Mach number by increasing the speed of sound), these two effects require a higher pressure in the chamber to obtain a correct mass flow rate. As the particles size chosen here were small compared to what should exist in the chamber, the pressure imposed within the combustion chamber led to underestimated gas mass flow in the computation.

In the following figures (Figure 6, Figure 7, Figure 8), the temperature ranges within the first cell of the plume are presented. At the lowest altitude (18.7 km), the end of the first cell is approximately 13 m behind the nozzle exit. At an altitude of 30 km, the first cell ends approximately 25 m after the nozzle exit, and at the highest altitude, the first cell ends approximately 60 m after the nozzle exit. Furthermore, the opening angle of the plume at the nozzle exit increases with increasing altitude. The reasons for this behaviour are first, the decreasing ambient pressure of the atmosphere with increasing altitude, and second, the increasing velocity of VEGA with increasing altitude. The second item is mainly responsible for the increasing length of the first cell with increasing altitude.

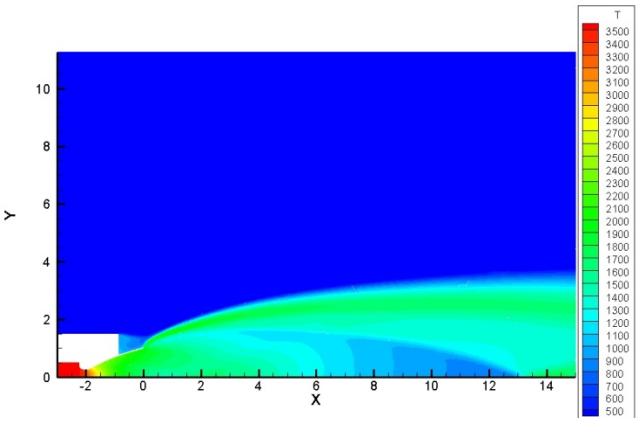

Figure 6: Temperature of the 1st cell (CFD) at 18.7 km

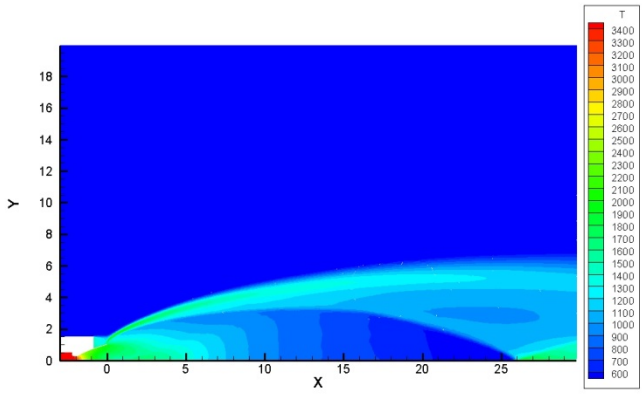

Figure 7: Temperature of the 1st cell (CFD) at 30 km

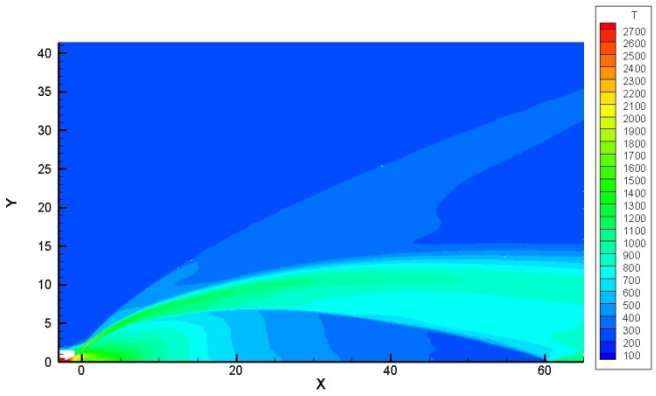

Figure 8: Temperature of the 1st cell (CFD) at 42 km

Afterburning which is a chemical reaction process is equivalent to increased OH concentration. The OH concentration of VEGA at an altitude of 30 km is shown in Figure 9. The analysis indicates that the afterburning mainly occurs in two areas: The shear layer beginning at the nozzle lip and the mixing layer several hundred meters after the nozzle exit.

However, the afterburning process strongly depends on the altitude and the velocity of the rocket. The tendency obtained by analysing the OH concentration is the faster the rocket, the higher the altitude and the lower the OH concentration and thus, the probability of afterburning.

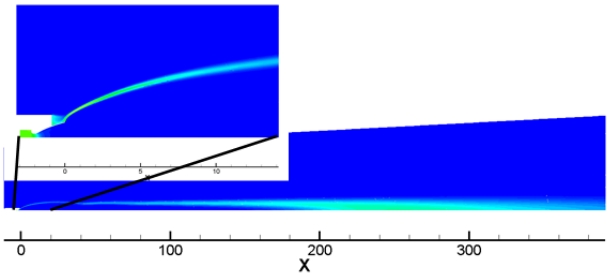

Figure 9: OH distribution at 30 km

5. Engineering Model Results

In the following section, the preliminary results of the engineering model for the inner plume flow for the first cell will be presented. Firstly, the mesh developed according to the above mentioned theory, will be shown, and secondly, the results for the static temperature will be demonstrated.

Mesh

In Figure 10 the mesh generated with the EM is shown. The blue lines indicate the characteristics C+ and the red lines indicate the characteristics C-. The region where the blue lines are dominant represents the area between the plume boundary and the barrel shock. Please note that the mesh for the EM is mirrored about the x-axis compared to the CFD.

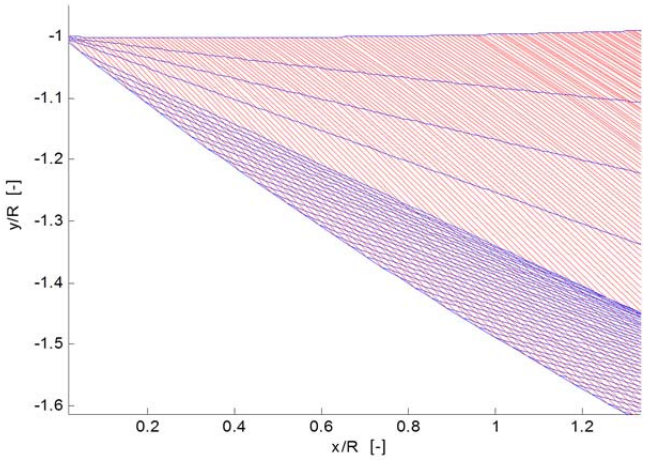

Figure 10: Mesh generated with the EM

First cell

In the following figures (Figure 11, Figure 12, and Figure 13), the temperature ranges within the first cell of the plume are presented. At the lowest altitude (18.7 km), the end of the 1st cell is approximately 14 m behind the nozzle exit. At an altitude of 30 km, the first cell ends approximately 25 m after the nozzle exit, and at the highest altitude, the first cell ends approximately 60 m after the nozzle exit. Also in the EM results, the opening angle of the plume at the nozzle exit increases with increasing altitude. At the 18.7 km altitude, the thickness is only a few meters whereas at the 42 km altitude, the thickness is around 12 m.

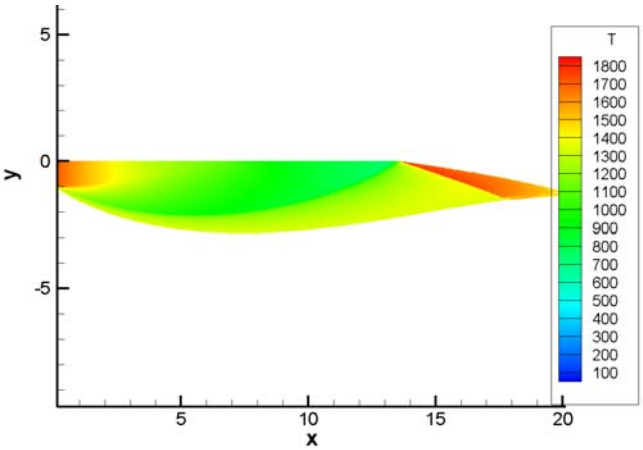

Figure 11: Temperature of the first cell (EM) at 18.7 km

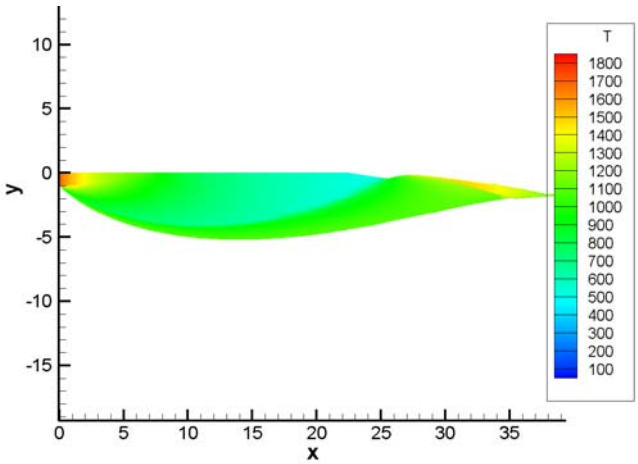

Figure 12: Temperature of the first cell (EM) at 30 km

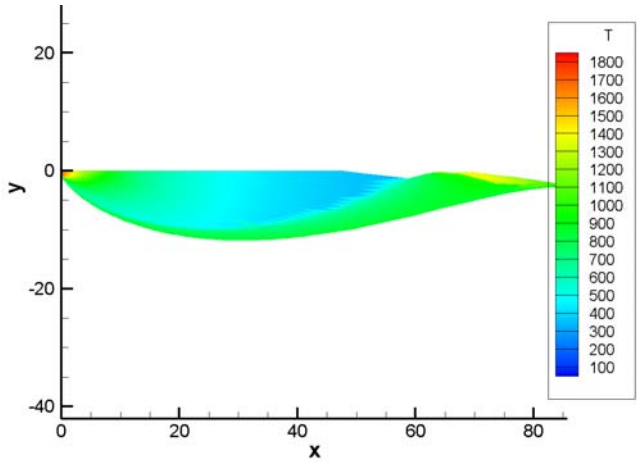

Figure 13: Temperature of the first cell (EM) at 42 km

6. Discussion

The results for VEGA for the three altitudes previously discussed are in good agreement between the EM and the CFD.

The following figures show the direct comparison between the CFD results and the results obtained by the EM for the altitude of 30 km.

Figure 14 displays the temperature ranges of the CFD (top) and the EM (below) at 30 km. It can be seen that the inner core has the same temperature ranges. Furthermore, the length of the first cell has the same length in both the CFD results and the EM results.

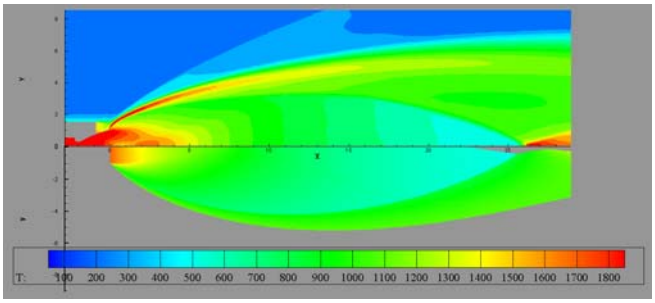

Figure 14: Comparison of the temperature between CFD (top) and EM (below) at 30 km

To summarize the results, it must be said that the values for the pressure and the temperature for the CFD and the EM are in the same order of magnitude. The values between the 2 sets of results vary due to the assumptions and simplifications that occur from the use of the method of characteristics in the EM.

The temperature and the shape of the plume of the EM are comparable with the results of the CFD and therefore, the EM will be further developed.

7. Conclusion & Outlook

For VEGA, the EM is verified by CFD results within the first cell. However, this is just the first step. The next steps are to implement the method of characteristics for the following cell and to implement the effects of afterburning for the EM.

Nevertheless, the EM is not being designed to completely replace CFD calculations, but to add the ability to achieve a basic level of information faster and for more altitudes then is currently able to be achieved with CFD alone.

Acknowledgement

The work described herein is funded by ESA through the General Studies Program under contract no. 4000105828/12/F/MOS. The project Atmospheric Impact of Launchers is part of the ESA CleanSpace Initiative.

References

[1] Dash, S. M., Wolf, D. E., *Fully-Coupled Analysis of Jet Mixing Problems Part I: Shock-Capturing Model, SCIPVIS*, NASA Contractor Report 3761, 1984

[2] Simmons, F. S., *Rocket Exhaust Plume Phenomenology*, The Aerospace Press, El Segundo, California, USA, 2000

[3] Dao, P. D., Farley, R., Soletsky, P., Gelbwachs, J., *LIDAR Measurements of the Stratospheric Exhaust Plume of Launch Vehicles*, 35th Aerospace Sciences Meeting & Exhibit, AIAA 97-0526. Aerospace Sciences Meeting, Reno, NV, USA, January 6-9, 1997

[4] Lohn, P. D., Wong, E. P., Smith Jr., T. W., *Rocket Exhaust Impact on Stratospheric Ozone*, TWR Space Electronic Group, 1999

[5] Smith, L. D., Edwards, J. R., Pilson, D., *Summary of the Impact of Launch Vehicle Exhaust and Deorbiting Space and Meteorite Debris on Stratospheric Ozone,* TRW Space and Electronics Group, 1999

[6] Burke, M. L., Zittel, P. F., *Laboratory Generation of Free Chlorine HCl under Stratospheric Afterburning Conditions*, Combustion and Flame, Vol. 112, No. 1-2, 1998

[7] Brady, B. B., Martin, L. R., Lang, V. I., *Effects of Launch Vehicle Emissions in the Stratosphere*, Journal of Spacecraft and Rockets, Vol. 34 (6), pp. 774–779.

[8] Denison, M. R.; Lamb, J. J.; Bjorndahl, E. Y.; Lohn, P. D.,*Solid Rocket Exhaust in the Stratosphere: Plume Diffusion and Chemical Reactions,* Journal of Spacecraft and Rocket, Vol. 31, No. 3, pp. 435–442, 1994

[9] Gomberg, R. I., Stewart, R. B., *A Computer simulation of the Afterburning Processes occurring within Solid Rocket Motor Plumes in the Troposphere*, , TN D-8303, 1976

[10] Leone, D. M., Turns, S. R., *Active Chlorine and Nitric Oxide Formation from Chemical Rocket Plume Afterburning*, 32nd Aerospace Science Meeting & Exhibition, Reno, NV, USA, January 10-13, 1994

[11] Anderson Jr., J. D., *Hypersonic and High-Temperature Gas Dynamics Second Edition*, AIAA, 2nd edition, November, 2006

[12] Vick, A. R., Andrews Jr., E. H., Dennard, J. S., Craidon, C. B., *Comparison of Experimental Free-Jet Boundaries with Theoretical Results obtained with the Method of Characteristics*, NASA Contractor Report, 1964

[13] Geuzaine, C., Remacle, J.-F., *GMSH: A Three-Dimensional Finite Element Mesh Generator with built-in Pre- and Post-processing Facilities*, International Journal for Numerical Methods in Engineering, Vol. 79 (11), pp. 1309-1331, 2009

[14] http://www.aerospacelab-journal.org , Issue 2, March 2011

[15] Turpin, G., Troyes, J., *Validation of a Two-Equation Turbulence Model for Axisymmetric Reacting and Non-Reacting Flows*, AIAA 2000-3463, 36th AIAA/ASME/SAE/ASEE Joint Propulsion Conference & Exhibit, Huntsville, AL, USA, July 17-19, 2000

[16] Troyes, J., Dubois, I., Borie, V., Boischot, A., *Multi-Phase Reactive Numerical Simulations of a Model Solid Rocket Motor Exhaust Jet*, 42nd AIAA/ASME/SAE/ASEE Joint Propulsion Conference & Exhibit, Sacramento, CA, USA, July 9-12, 2006